

A global climatology of stratospheric aerosol size distribution parameters derived from SAGE II data over the period 1984–2000: 1. Methodology and climatological observations

Christine Bingen, Didier Fussen, and Filip Vanhellemont

Belgian Institute for Space Aeronomy, Brussels, Belgium

Received 20 February 2003; revised 26 June 2003; accepted 31 October 2003; published 19 March 2004.

[1] A global climatology has been derived for different parameters characterizing the size distribution of stratospheric aerosols; the particle number density, median radius, and mode width of the particle distribution were assumed to be lognormal. Those parameters were retrieved by applying an original optical inversion scheme on Stratospheric Aerosol and Gas Experiment (SAGE) II aerosol extinction profiles spanning from 1984 to 2000. The specificity of the inversion algorithm resides in the use of a continuity constraint that allows one to partly get rid of the ill-posedness of the inversion problem and to greatly improve the quality and the stability of the solution. The long time period covered by the SAGE II experiment allows us to observe very different situations of volcanic load, from highly volcanic periods following major eruptions (mainly after the Pinatubo eruption of June 1991), to periods of very low aerosol load. Beyond the effects of volcanism on the aerosol parameters, other influences are observed such as seasonal effects, more particularly at midlatitude. Also the quasi-biennial oscillation (QBO) shows a clear influence on the size distribution. In this paper, we present the general features of the different aerosol profiles, and we investigate the effects of these three main influences affecting the size distribution. We present the climatology in a more quantitative way in a companion paper, by proposing reference data for the three considered aerosol parameters.

INDEX TERMS: 0305 Atmospheric Composition and Structure: Aerosols and particles (0345, 4801); 0340 Atmospheric Composition and Structure: Middle atmosphere—composition and chemistry; 0370 Atmospheric Composition and Structure: Volcanic effects (8409);

KEYWORDS: stratospheric aerosols, aerosol climatology, aerosol size distribution

Citation: Bingen, C., D. Fussen, and F. Vanhellemont (2004), A global climatology of stratospheric aerosol size distribution parameters derived from SAGE II data over the period 1984–2000: 1. Methodology and climatological observations, *J. Geophys. Res.*, 109, D06201, doi:10.1029/2003JD003518.

1. Introduction

[2] Because of their influence on the radiation transfer properties and to their importance in the physico-chemistry of the atmosphere, aerosols are constituents of major importance in the stratosphere. Therefore a reliable characterization of their properties is necessary for a correct understanding and modeling of the atmospheric processes. However, because of their great natural variability, the characterization of aerosol behavior remains a complex problem. Among other difficulties, the aerosol density range can change by 2 orders of magnitude or more between periods of very high volcanic load following an event such as the Pinatubo eruption in June 1991, and time periods of very low aerosol mass load. Moreover, the spatiotemporal evolution of aerosol spread due to transport is strongly influenced by seasonal effects, and hence by the geolocation and the time of the year at which volcanic injection of aerosol occurs in the stratosphere [Hofmann, 1988].

[3] During the two last decades, our knowledge about aerosols and their impact on the atmospheric physico-chemistry has appreciably improved [Russell *et al.*, 1996], thanks to the refinement of remote sensing techniques [Stein *et al.*, 1994; Thomason *et al.*, 1997; Lambert *et al.*, 1997; Randall *et al.*, 2000; Berthet *et al.*, 2002] and of in situ measurements [Goodman *et al.*, 1994; Pueschel *et al.*, 1994; Sugita *et al.*, 1999; Deshler, 1994, and references therein]. The evolution of aerosol properties after the eruptions of El Chichon and mainly of Pinatubo was intensively observed and studied [Tie *et al.*, 1994; Zhao *et al.*, 1995; Brogniez *et al.*, 1996], and several works were devoted to the description of stratospheric aerosols over large timescales [Hitchman *et al.*, 1994; Thomason *et al.*, 1997; Fussen and Bingen, 1999; Bingen and Fussen, 2000].

[4] Nevertheless, quantitative data and long term trends still remain difficult to derive on a global scale for aerosol parameters such as the aerosol particle number density. In situ measurements provide vertical profiles with a good accuracy, with detailed information about local air mass characteristics and displacements, but remain local. On the other hand, remote sensing gives a global insight of the

aerosol properties, but fundamental limitations of scattering measurements in the Rayleigh limit makes the discrimination of very small particles impossible. Furthermore, because of the ill-conditioned character of the optical inversion, the derivation of aerosol parameters from extinction profiles may lead to unstable solutions and to strong correlations between the retrieved aerosol parameters, depending, e.g., on the experimental signal to noise ratio [Echle *et al.*, 1998]. For this reason, climatologies of aerosols are in most cases dealing with integrated parameters like the effective radius or the surface area density. It is worth to mention in this context that the last version (6.1) of Stratospheric Aerosol and Gas Experiment (SAGE) II contains aerosol surface area density profiles for all valid events. Unfortunately, the retrieval algorithm of these data has not been published so far. The retrieval of the particle density is much less easy, and as long as we know, no climatology of aerosol density profiles has been proposed so far for this parameter.

[5] Recently, we investigated the optical inversion problem, and proposed a regularized inversion method in order to enhance the stability and the reliability of the aerosol parameter retrieval [Fussen *et al.*, 2001a; Bingen *et al.*, 2002]. This method allows one to derive the particle number density, and the modal parameters of a lognormal particle size distribution. We applied this inversion method to extinction profiles supplied by the SAGE II experiment launched in October 1984. In this way, we obtained profiles on a near global scale for the three considered aerosol parameters, covering the whole time period 1984–2000. The aim of the present paper is to investigate a climatology of aerosols based on the inverted SAGE II profiles. After a description of the basic data set and of the optical inversion method, we study the spatiotemporal evolution of aerosol distribution during 16 years of SAGE II mission involving several major volcanic eruptions, and mainly the Pinatubo eruption in June 1991 and the whole relaxation period following this event. The effect of seasonal cycles on the aerosol spread is illustrated for both hemispheres, and more precisely the annual cycles at midlatitudes, governed by variations of the polar vortex. Also the influence of the quasi-biennial oscillation (QBO) on the three considered parameters is investigated, in relation with previous studies concerning other aerosol parameters of interest. In a companion paper, we try to discern the influence of volcanism and the contribution of seasonal effects. We quantify the evolution of the aerosol parameters during the relaxation of volcanic loading after a major eruption, as well as the deviation from this evolution due to other effects [Bingen *et al.*, 2004a]. We complete this quantitative study by a presentation of the error found on the different aerosol parameters and by an overview of our validation work.

2. SAGE II Data Set

[6] The original data set consists of the aerosol extinction profiles provided by the Stratospheric Aerosol and Gas experiment II (SAGE II) at wavelengths $\lambda = 1.020, 0.525, 0.453$ and $0.385 \mu\text{m}$ [Chu *et al.*, 1989]. Those vertical profiles extend formally from 0 to 50 km, although only the $1.020 \mu\text{m}$ is able, in case of a clear atmosphere, to reach the ground level. This is due to the cutoff frequency in the UV

region, affecting the other spectral channels. The data set covers the (80°S – 80°N) latitude range from October 1984 to March 2000. We used here the version 6.0 which presents significant changes with respect to the previous versions, induced by a better estimation of the altitude. The error calculation was also improved. Information about this version is available on the website of SAGE II <http://www-sage2.larc.nasa.gov>). A comparison of the aerosol parameters retrieved by our optical inversion method from the version 6.0 and from the previous version 5.931 shows indeed an appreciable enhancement of the retrieved parameters, with, for instance, the disappearance of unrealistically high values of the median radius at high altitudes.

3. Inversion Method

[7] The inversion method we used to retrieve the various aerosol parameters has been presented previously [Bingen *et al.*, 2002]. The basic problem consists in the inversion of the expression describing the extinction coefficient β due to a population of small aerosol droplets:

$$\beta(z; \lambda) = \int_0^{+\infty} N(z) f(r, z) Q(r; \lambda) dr \quad (1)$$

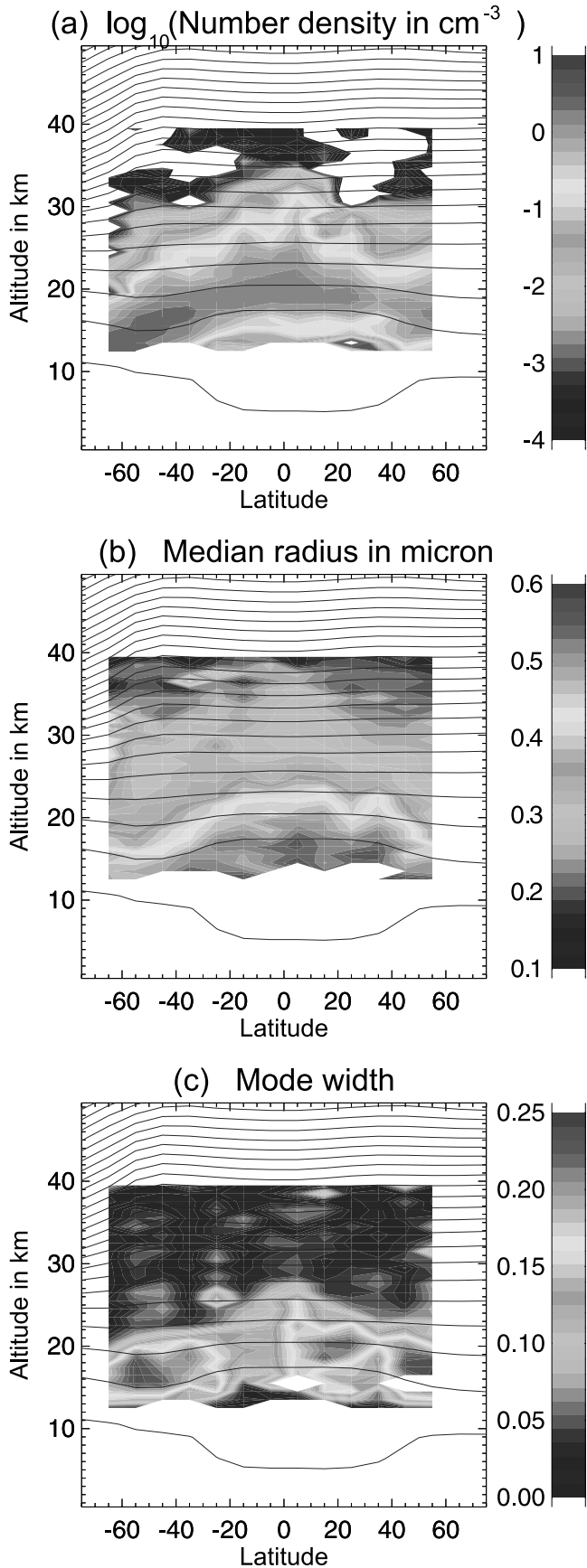
[8] In this relation, $N(z)$ represents the total particle number density at altitude z , $f(r, z)$ is the particle size distribution and $Q(r; \lambda)$ is the extinction cross section depending on the wavelength λ , the particle radius r and the refractive index. The particles are supposed to be spherical, so that $Q(r; \lambda)$ can be calculated from the Mie scattering theory [van de Hulst, 1957]. Volcanism is known to be the dominating process in aerosol formation in the stratosphere. Although recent studies suggest the presence of soot in the lower stratosphere up to altitudes exceeding 20 km [Renard *et al.*, 2002], stratospheric aerosols are generally assumed to be a mixture of about 75% H_2SO_4 and 25% H_2O wt, characterized by a purely real refractive index of 1.43 in the UV-visible and near infrared SAGE II wavelength range.

[9] The particle size distribution is usually expressed as a lognormal function

$$f(r) = \frac{1}{\sqrt{2\pi}r\sigma} \exp\left(-\frac{\ln^2(r/\rho)}{2\sigma^2}\right) \quad (2)$$

with median radius ρ and mode width σ . During periods of high volcanism, the aerosol size distribution is proved to be better described by bimodal [Deshler *et al.*, 1993; Stone *et al.*, 1993; Goodman *et al.*, 1994] or even trimodal [Pueschel *et al.*, 1994] size distributions, that better take into account the coexistence of particle populations of different origins: tiny droplets of fresh aerosol, aerosol particles growing on preexisting condensation nuclei, ashes. However, we have not considered multimodal distributions in this work, because of the limited number of SAGE II spectral channels, restricting too severely the amount of available information.

[10] The optical inversion problem consists in retrieving the aerosol parameters $N(z)$, $\rho(z)$, $\sigma(z)$ from equations (1) and (2) by using the experimental extinction profiles as input data for the left-hand side of equation (1). The



parameter $N(z)$ can be easily eliminated by a proper normalization of the problem using reduced extinction coefficient

$$\beta_n = \frac{\beta(z; \lambda)}{\beta(z; \lambda_r)} \quad (3)$$

In this work, we used the $1.020 \mu\text{m}$ SAGE II channel as reference wavelength λ_r . This channel provides the most accurate extinction profiles and is characterized by the greatest penetration depth into the atmosphere, as already mentioned.

[11] Using a wide set of ρ and σ values, we computed theoretical values of β_n using the Mie theory in order to build up a lookup table of theoretical values $\beta_n^t(\rho, \sigma; \lambda)$. The inversion problem was then solved by minimizing the merit function

$$M(\rho, \sigma; z) = \sum_{i=1}^3 \left[\frac{\beta_n^e(z; \lambda_i) - \beta_n^t(\rho, \sigma; \lambda_i)}{\Delta\beta_n^e(z; \lambda_i)} \right]^2 \quad (4)$$

describing the difference between the theoretical values $\beta_n^t(\rho, \sigma; \lambda)$ and the experimental extinction profiles normalized according to equation (3), $\beta_n^e(z; \lambda_i)$. The difference between both profiles is weighted by the estimated error $\Delta\beta_n^e(z; \lambda_i)$ on β_n^e and the sum is taken over the different SAGE II wavelengths. In order to reduce the ill-posedness of the inversion problem [Echle *et al.*, 1998; Fussen *et al.*, 2001a; Bingen *et al.*, 2002] and hence to enhance the stability of the solution in ρ and σ , we constrained the problem by imposing a smoothness condition in the altitude on both parameters:

$$\rho(z) = \rho_{\min} + (\bar{\rho} - \rho_{\min}) \exp \left[- \left(\sum_{i=0}^{n-1} a_i z^i \right)^2 \right] \quad (5)$$

$$\sigma(z) = \sigma_{\min} + (\bar{\sigma} - \sigma_{\min}) \exp \left[- \left(\sum_{i=0}^{n-1} b_i z^i \right)^2 \right] \quad (6)$$

In these expressions, the maximum values $\bar{\rho}, \bar{\sigma}$ are constrained within the working ranges $[\rho_{\min}, \rho_{\max}]$ and $[\sigma_{\min}, \sigma_{\max}]$ respectively.

[12] A value $n - 1 = 3$ for the polynomials degree in equations (5) and (6) was found to be a good trade-off between reduction of the vertical resolution, stability of the solution, and computing time. This value of n is high enough to allow a suitable reproduction of the general structure of the aerosol distribution in the stratosphere. The choice of a continuous function prevents possible occurrence of isolated unrealistic values in the aerosol profiles due to a local fail of the optimization algorithm. On the other side, this formulation do not allow the

Figure 1. Mean dependence in latitude and altitude of the three aerosol parameters of interest, for September 1993: (a) particle number density, (b) median radius, and (c) mode width. The contour lines represent isentropic lines. See color version of this figure at back of this issue.

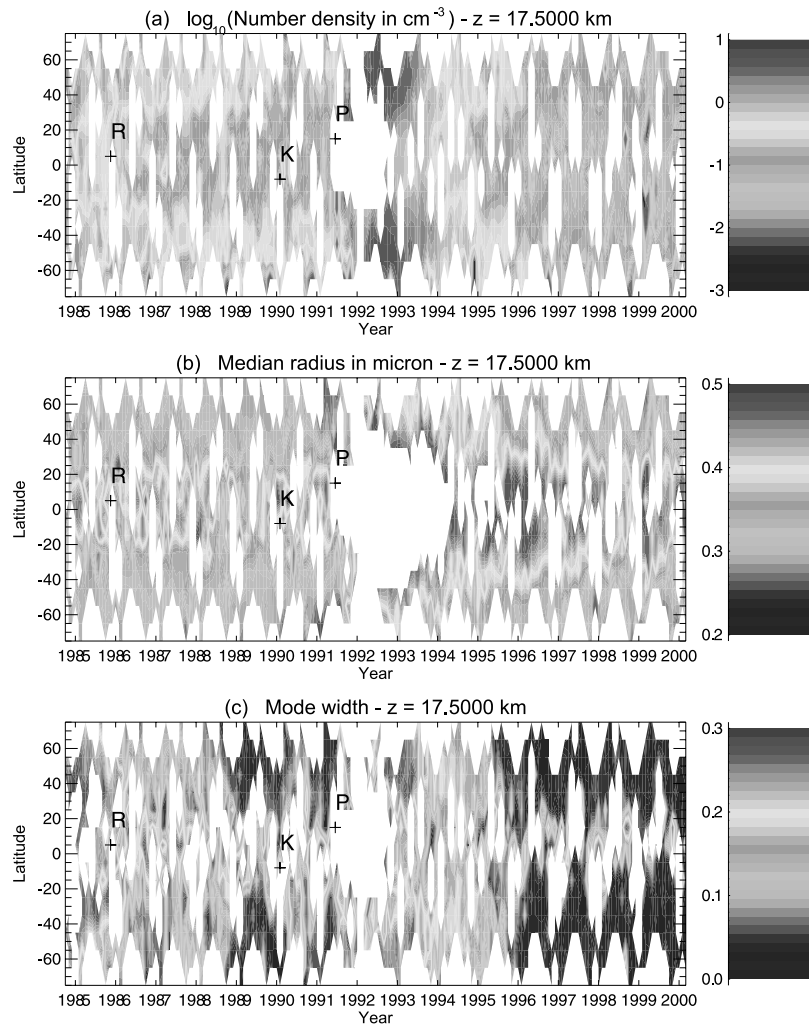


Figure 2. Mean dependence in time and latitude of the aerosol parameters of interest, at $z = 17.5$ km: (a) particle number density, (b) median radius, and (c) mode width. See color version of this figure at back of this issue.

reproduction of fine structures or local perturbations of the aerosol profiles, such as the influence of local inclusions of air masses coming from other latitudes and characterized by different microphysical features.

[13] After injecting equations (5) and (6) into equation (4), the problem comes down to find values of $\bar{\rho}$, $\bar{\sigma}$, a_i and b_i which minimize the merit function of the constrained problem

$$M^c(\bar{\rho}, \bar{\sigma}; a_i, b_i) = \sum_z M(\rho(z; \bar{\rho}; a_i), \sigma(z; \bar{\sigma}; b_i); z) \quad (7)$$

The minimization was performed by using a standard Levenberg-Marquardt algorithm.

[14] Finally, the particle number density N is retrieved by injecting the solutions in ρ , σ into the original problem (equation (1)) using equation (2).

[15] For practical use, binned profiles were computed from all $\rho(z)$, $\sigma(z)$ and $N(z)$ profiles, using time and latitude intervals of respectively one month and 10 degrees. The altitude is given with a resolution of 1 km. The binning results in mean profiles representative for the aerosol content of each considered bin, out of very local perturba-

tions in time and latitude or sudden changes of the aerosol profiles. Notice that we refer to each latitude bin, on the graphical representations, by their middle value.

4. Validity Range of the Climatological Data Set

[16] Several intercomparisons have been performed in previous works to validate the climatology presented here [Bingen *et al.*, 2002, 2003, 2004b]. We propose an overview of all these efforts in the companion paper [Bingen *et al.*, 2004a] and we will restrict ourselves, here, to mention briefly the main factors likely to increase the error in the climatological data set.

[17] One error factor concerns the inability of spectral measurement techniques such as those used by SAGE II to discriminate thin particles in the Rayleigh limit of scattering. It is well known that the extinction cross section $Q(r; \lambda)$ simplifies, when the particle size r is small with respect to the wavelength λ , into an expression which only depends on λ and no more on r . In this case, the extinction measurement does not contain any information about the particle size.

[18] Another limitation concern the hypothesis made in the previous section concerning the monomodal and log-

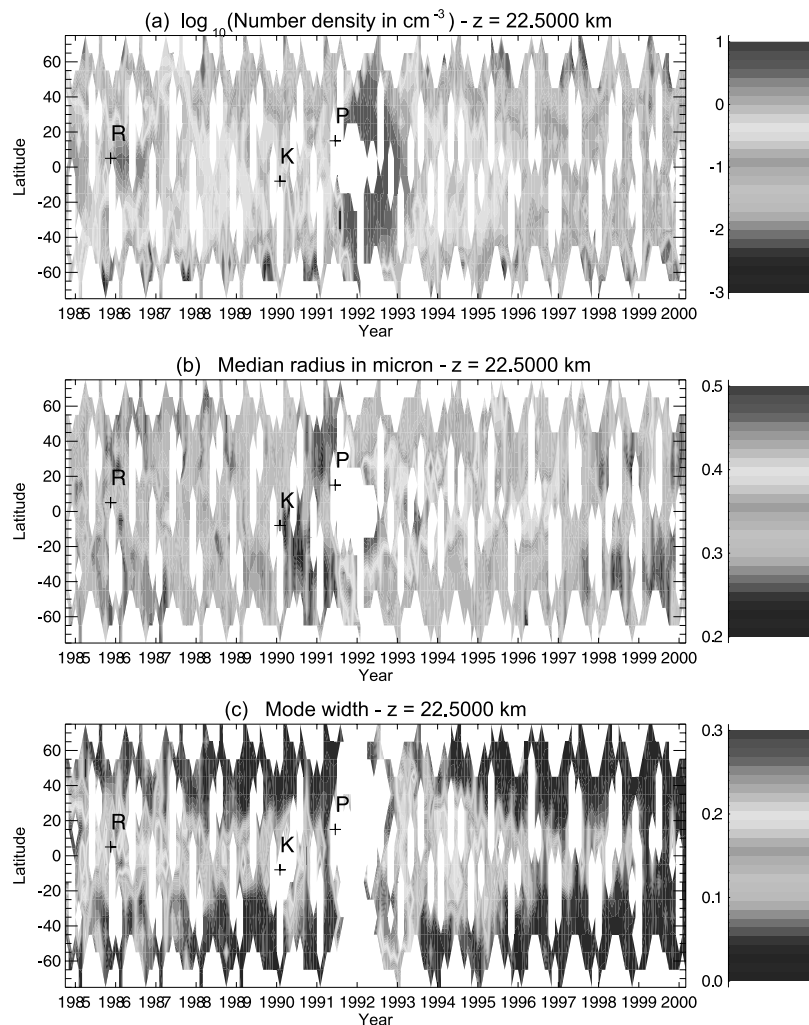


Figure 3. Same as Figure 2, at $z = 22.5$ km. See color version of this figure at back of this issue.

normal character of the particle size distribution. As already mentioned, the aerosol population during periods of high volcanism is characterized by the presence of particles from different origins, with quite different microphysical features. Even out of those periods, bimodal size distributions can be more adapted to describe the particle population and other choice than the lognormal distribution may be more adapted, especially in the lowermost stratosphere [Berthet *et al.*, 2002; Renard *et al.*, 2002].

[19] As a consequence, we expect the performances of the climatology to decrease in situations where very thin par-

ticles ($r \leq 0.2$ to $0.3 \mu\text{m}$) dominate the particle population, and when the coexistence of several particle modes make the choice of a monomodal size distribution inadequate.

5. General Features of the Latitudinal Aerosol Profile

[20] Typical profiles for particle number density, median radius and mode width retrieved from SAGE II and binned as described previously, are shown in Figure 1. They concern the month September 1993 characterized by a

Table 1. Occurrence of the Westerly Shear of the QBO at Various Altitudes During the Time Period 1984–2000^a

$z = 24$ km	$z = 26$ km	$z = 30$ km
Nov. 1984 to May 1986	Sept. 1984 to Oct. 1985	June 1984 to July 1985
July 1987 to March 1989	June 1987 to Feb. 1988	April 1987 to Feb. 1988
Feb. 1990 to April 1991	Nov. 1989 to March 1991	July 1989 to July 1990
Nov. 1992 to June 1993	Sept. 1992 to May 1993	Oct. 1992 to April 1993
Dec. 1994 to June 1995	Oct. 1994 to June 1995	Oct. 1994 to March 1995
April 1997 to July 1997	Dec. 1996 to June 1997	Nov. 1996 to May 1997
Feb. 1999 to June 1999	Nov. 1998 to April 1999	Nov. 1998 to Feb. 1999

^a The reference latitude is 5°N . The presented data were partly taken from Holton [1992] and partly derived from climatological wind fields supplied by the United Kingdom Meteorological Office (UKMO).

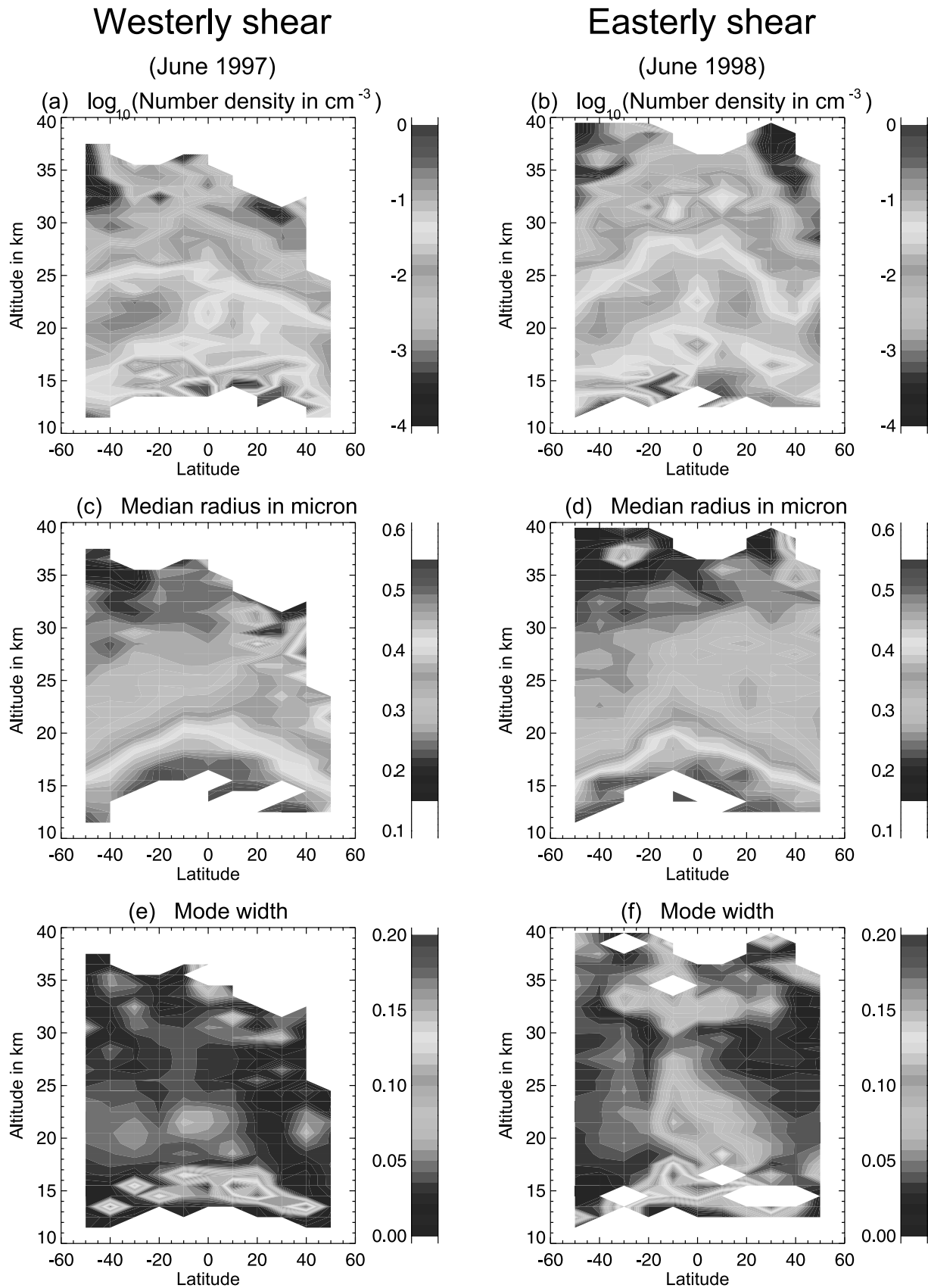


Figure 4. Influence of the QBO on the aerosol parameter profiles. (a and b) $\text{Log}_{10}(N)$; (c and d) median radius; (e and f) mode width. The profiles concern the months June 1997 and June 1998, taking place in two consecutive phases of the QBO, respectively the westerly and easterly shear. See color version of this figure at back of this issue.

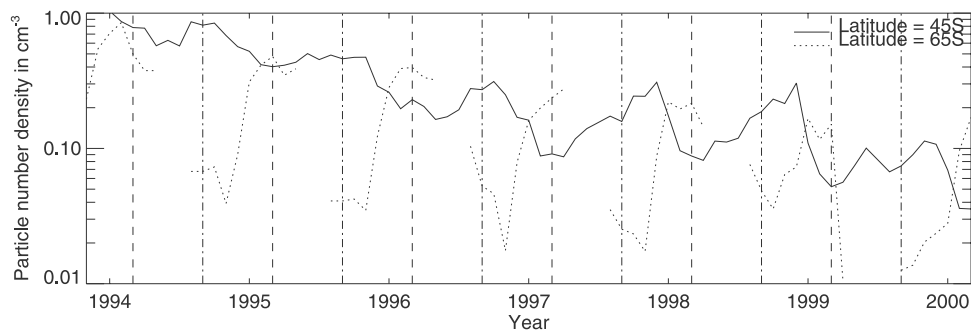


Figure 5. Temporal evolution of the particle number density between 50°S and 40°S (solid line) and between 70°S and 60°S (dotted lines), from November 1993 to March 2000, at $z = 17.5$ km. Vertical lines correspond to the months of March (dashed lines) and September (dot-dashed lines). The curves were filtered using a three-month sliding window.

medium volcanic aerosol load. Their structure follows the well known general latitudinal patterns already described in the literature [Hitchman *et al.*, 1994; Trepte *et al.*, 1994].

[21] The three profiles show an elevation of the aerosol layer in the intertropical region, representative of the strong upward streams inducing a mass transfer from the troposphere to the stratosphere and giving rise to an aerosol reservoir in the equatorial region. Above 20 km, the three aerosol parameters of interest take, for a given altitude, their maximal values at central latitudes. This mode of transport corresponds to the upper regime defined by Hitchman *et al.* [1994], and whose strength is known to depend on the phase of the QBO. At midlatitudes, the aerosol undergoes a poleward transport which gives rise to profiles which are roughly parallel to the isentropics at midlatitudes for all aerosol parameters (the lower regime, following Hitchman *et al.*'s denomination).

[22] The transport is essentially perturbed in zones where the potential vorticity is enhanced, giving rise to a local barrier inhibiting the poleward aerosol dispersion. It is the case in the subtropical regions above 20 km, where a strong meridional gradient is observed on the N , ρ and σ profiles due to the occurrence of the easterly phase of the QBO at this time. Around 60° latitude, the polar vortex creates a barrier obstructing the transport to higher latitudes and inducing a local subsidence of aerosol just above the tropopause. Because of the accumulation of aerosol mass, the particle number density and the dispersion of the size distribution increases. The influence of the QBO and seasonal influences will be discussed with more detail below. Consecutively to the Pinatubo eruption, the highest

values for N and σ are reached after about 12 to 18 months at 60° latitude, whereas the increasing period for the same parameters does not exceed 6 months at the equator (see Figures 2a and 3a). It is also interesting to notice the asymmetry in the particle number density clearly visible in Figure 1a, denoting a more important transport to the southern hemisphere below 20 km. The evidence of a southward tongue in the aerosol layer has already been mentioned in the literature [Thomason *et al.*, 1997; Weisenstein *et al.*, 1997; Fussen *et al.*, 2001b]. Above 25 km altitude, this marked asymmetry is not observed anymore.

[23] The influence of major volcanic eruptions (El Chichon, 17°N, November 1982; Ruiz, 5°N, November 1985, Kelut, 8°S, February 1990, Pinatubo, 15°N, June 1991 and Hudson, 46°S, August 1991) is well illustrated in Figures 2 and 3, showing the evolution in time and latitude of the three aerosol parameters at altitudes of 17.5 km and 22.5 km. On all these figures, missing data are related to zones not covered by the SAGE II experiment due to orbital characteristics, or whose value stands out of the chosen color scale. An exception is the region common to the three subplots, at the central latitudes, where an important lack of data is observed from mid-1991 to 1993. This latest case is related to the highly loaded atmosphere after the Pinatubo eruption, preventing any measurement within the sensitivity range of the instrument.

[24] The formation of an accumulation zone at midlatitude following major eruptions is clearly visible in Figures 2a and 2c. At these latitudes, N and σ take higher values than in the equatorial region. This concerns the lowermost stratosphere and such an accumulation zone is

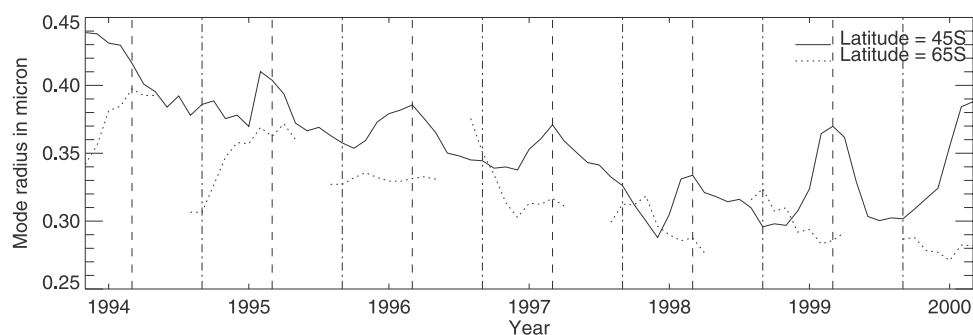


Figure 6. Same as Figure 5, for the median radius ρ .

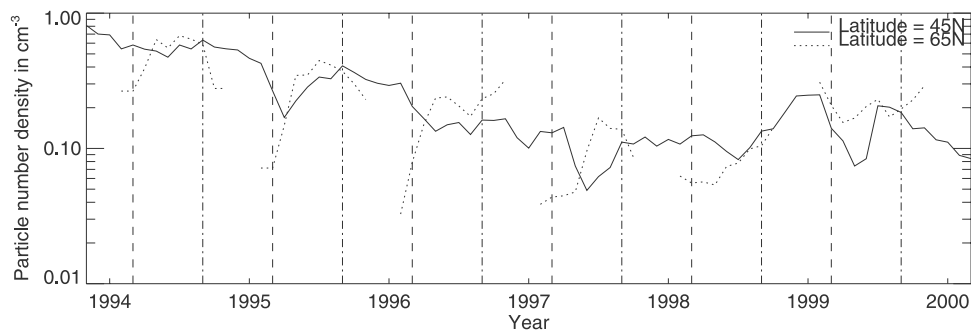


Figure 7. Temporal evolution of the particle number density between 40°N and 50°N (solid line) and between 60°N and 70°N (dotted lines), from November 1993 to March 2000, at $z = 17.5$ km. Vertical lines correspond to the months of (dashed lines) and September (dot-dashed lines). The curve was filtered using a three-month sliding window.

not observed above 20 km (see Figures 3a and 3c). Notice that, contrarily to N and σ , the median radius ρ does not take maximal values in the accumulation zone, but well in the tropical region, as can be seen in Figure 2b. Nevertheless, the Pinatubo eruption has a noticeable influence on the median radius profile, broadening significantly the aerosol reservoir after the eruption below 20 km. The spread of the reservoir then progressively decreased before reaching a rather stable value after about 30 months. It is interesting to notice that this new apparently stable structure is quite broader than the median radius profile prior to the Pinatubo eruption, and keeps this characteristic during at least 7 years after the eruption.

[25] Above 25 km, the latitudinal variability of the aerosol parameters decreases appreciably, and except at transient periods following volcanic eruptions (not illustrated here), they do not present any pronounced latitudinal dependence. Notice that the influence of the Pinatubo is still visible above 30 km two year after the eruption, leading to an increase of about 2 orders of magnitude of the particle number density with respect to the value before the eruption.

6. Influence of the QBO

[26] The quasi-biennial oscillation, characterized by an inversion of the dominant zonal wind with a period of about 24 to 30 months, is a phenomenon which affects the circulation mainly in the lower tropical atmosphere [Baldwin *et al.*, 2001]. However, the perturbations induced

in the circulation have perceptible consequences at higher latitudes. The wind inversion occurs from an altitude of 30 km, and gradually goes down to about 23 km. At this altitude, the wave is rapidly attenuated. The occurrence of the westerly shear at several altitudes is indicated in Table 1 for the time period covering the duration of the SAGE II experience.

[27] As already noticed by Hitchman *et al.* [1994], the QBO has a significant influence on the aerosol distribution. The authors observed a lofting and gathering of the extinction contours during the easterly shear, and a subsidence and widening of the zone of high extinction coefficient due to descending air motion associated with the westerly phase of the QBO.

[28] The influence of QBO on the aerosol parameter profiles is illustrated in Figure 4. The three aerosol parameters are represented as a function of latitude and altitude, in June 1997 and June 1998. Those months are respectively situated within the easterly and westerly shear of the QBO, during a period of low volcanic loading in the atmosphere. The choice of the same month in both cases allows one to get rid of any seasonal effects, so that the QBO appears to be the most important factor influencing the profiles.

[29] During the easterly shear (Figures 4b, 4d, and 4f), the high values of N , ρ and σ found above the tropical reservoir reveals the presence of strong ascending fluxes, and the lofting and gathering effects occurring within the intertropical region is well observed on the three parameters profiles. On the other hand, the contour lines in Figures 4a, 4c, and 4e illustrating the westerly shear show an enhanced

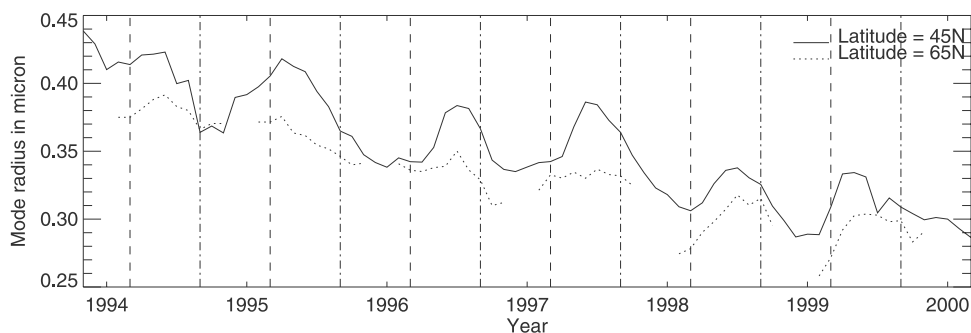


Figure 8. Same as Figure 7, for the median radius ρ .

poleward mass displacement, in agreement with Hitchman *et al.*'s [1994] observations that this phase of the QBO favors the lower regime and aerosol mass displacement by this way.

7. Seasonal Effects

[30] The general circulation shows strong annual variations at middle and high latitude [Brasseur *et al.*, 1999; Holton, 1992] governed by the temperature gradients that appear between the equatorial and polar regions. These gradients result in strong zonal winds whose speed and direction varies during the year. Easterly winds are observed in the summer hemisphere, and westerlies in the winter hemisphere. The maximum speed is reached around the solstices, and the polar vortex forms a barrier for poleward mass drift at these periods of the year. The wind direction reverses from West to East after the equinoxes, around March–April in the northern hemisphere, and around October–November in the southern hemisphere. The polar vortex then breaks up, allowing transport of species from midlatitudes to the poles. Because of the more pronounced structures of the orography in the northern hemisphere, the polar vortex tends to break up more easily in this hemisphere, whereas it is more stable and characterized by stronger zonal winds in the southern hemisphere. An asymmetry between both hemispheres is also observed in the meridional circulation, with a more vigorous circulation in the winter hemisphere and especially in the southern hemisphere, due to the enhanced temperature gradient between tropical and polar regions.

[31] The effects of this seasonal influence are found again in the annual variations of the aerosol parameters N , ρ and σ . Because of the possibly high random variations, those oscillations may be difficult to observe directly, but the data filtering by a three-month sliding window allows one to sensibly reduce the random variations, revealing clearly annual cycles that are particularly marked in the lower stratosphere.

[32] The time evolution of N and ρ at 17.5 km altitude filtered in this way is shown in Figures 5–8 for the post-Pinatubo period. It illustrates clearly the influence of the polar vortex on the aerosol dispersal to the poles. During the fall and winter in the southern hemisphere, N increases at midlatitude and simultaneously decreases strongly beyond the polar jet barrier. During summer, consecutively to the break up of the polar vortex, N decreases significantly around 40 to 50°, whereas a rapid increase is observed at high latitudes during the same period.

[33] In the northern hemisphere, N shows similarly a rapid decay at the end of the winter. During spring and summer, N decreases at 40° to 50° and simultaneously, increases noticeably at high latitudes (see Figure 7). Nevertheless, the characteristics of the dynamics in this region lead to some differences in the aerosol evolution with respect to the southern hemisphere. The seasonal cycles are less marked and more irregular, and the increasing phase of N at midlatitudes is short-lived with respect to the equivalent period in the southern hemisphere.

[34] During those seasonal cycles, the variations of N can range from a factor of 3 to more than 1 order of magnitude.

[35] In both hemispheres, the median radius shows a very clear seasonal cycle during which, at 40° to 50°, ρ increases whereas N decreases. The median radius ρ takes its maximal value at the beginning of the fall in the southern hemisphere and during the summer in the northern hemisphere. Lower values of ρ are found during the winter and spring in both hemispheres, although more variability is observed in this annual cycle. These typical variations of N and ρ concern essentially the lower stratosphere. They are not observed at altitudes higher than 22 km.

8. Conclusions

[36] We presented a climatology of aerosol parameters derived by optical inversion of SAGE II extinction profiles. This climatology concerns the particle number density, the median radius and the mode width of an assumed equivalent lognormal size distribution.

[37] From these data, we illustrated the influence of seasonal effects and more precisely of the polar vortex on the aerosol evolution during the year. Also the effects of QBO were investigated, leading to the observation of typical patterns for N , ρ and σ looking similar to the structures already found in previous studies for other aerosol parameters.

[38] A further step of this work is to quantify the spatiotemporal evolution, in order to dispose on realistic values for the different parameters on interest and to evaluate the respective influences of volcanism and dynamical effects. This aspect is treated in a twin paper, where we try to derive reference values of N , ρ and σ representative for the whole relaxation period following a volcanic eruption of major importance, on the basis of the Pinatubo eruption in June 1991.

[39] **Acknowledgments.** This work was supported by the Federal Office for Scientific, Technical and Cultural Affairs, under grant MO/35/004. The SAGE II data were obtained from the NASA Langley Research Center EOSDIS Distributed Archive Center.

References

- Baldwin, M. P., et al. (2001), The quasi-biennial oscillation, *Rev. Geophys.*, *39*, 179–229.
- Berthet, G., et al. (2002), Optical and physical properties of stratospheric aerosols from balloon measurements in the visible and near-infrared domains. I. Analysis of aerosol extinction spectra from the AMON and SALOMON balloonborne spectrometers, *Appl. Opt.*, *36*, 7522–7538.
- Bingen, C., and D. Fussen (2000), Structure and spectral features of the stratospheric aerosol extinction profiles in the UV-visible range derived from SAGE II data, *J. Geophys. Res.*, *105*, 4767–4776.
- Bingen, C., F. Vanhellefont, and D. Fussen (2002), A new regularized inversion method for the retrieval of stratospheric aerosol size distributions applied to 16 year SAGE II data (1984–2000): Method, results and validation, *Ann. Geophys.*, *21*, 797–804.
- Bingen, C., D. Fussen, and F. Vanhellefont (2003), Characterization of stratospheric aerosol distribution for volcanic and non volcanic aerosols observed through 16 years of SAGE II data (1984–2000), in *Volcanism and Earth's Atmosphere*, *Geophys. Monogr. Ser.*, vol. 139, edited by A. Robock and C. Oppenheimer, pp. 93–105, AGU, Washington, D. C.
- Bingen, C., D. Fussen, and F. Vanhellefont (2004a), A global climatology of stratospheric aerosol size distribution parameters derived from SAGE II data over the period 1984–2000: 2. Reference data, *J. Geophys. Res.*, *109*, D06202, doi:10.1029/2003JD003511.
- Bingen, C., D. Fussen, and F. Vanhellefont (2004b), A global climatology of stratospheric aerosols using SAGE II data: Toward a systematic characterization of the aerosol evolution, *Adv. Space Res.*, in press.
- Brasseur, G. P., J. J. Orlando, and G. S. Tyndall (Eds.) (1999), *Atmospheric Chemistry and Global Change*, Oxford Univ. Press, New York.

- Brogniez, C., J. Lenoble, M. Herman, P. Lecomte, and C. Verwaerde (1996), Analysis of two balloon experiments in coincidence with SAGE II in case of large stratospheric aerosol amount: Post-Pinatubo period, *J. Geophys. Res.*, *101*, 1541–1552.
- Chu, W. P., M. P. McCormick, J. Lenoble, C. Brogniez, and P. Pruvost (1989), SAGE II inversion algorithm, *J. Geophys. Res.*, *94*, 8339–8351.
- Deshler, T. (1994), In situ measurements of Pinatubo aerosol over Kiruna on four days between 18 January and 13 February 1992, *Geophys. Res. Lett.*, *21*, 1323–1326.
- Deshler, T., B. J. Johnson, and W. R. Rozier (1993), Balloonborne measurements of the Pinatubo aerosol during 1991 and 1992 at 41°N: Vertical profiles, size distribution, and volatility, *Geophys. Res. Lett.*, *20*, 1435–1438.
- Echle, G., T. von Clarmann, and H. Oelhaf (1998), Optical and microphysical parameters of the Mt. Pinatubo aerosol as determined from MIPAS-B mid-IR limb emission spectra, *J. Geophys. Res.*, *103*, 19,193–19,211.
- Fussen, D., and C. Bingen (1999), A volcanism dependent model for the extinction profile of stratospheric aerosols in the UV-visible range, *Geophys. Res. Lett.*, *26*, 703–706.
- Fussen, D., F. Vanhellemont, and C. Bingen (2001a), Evolution of stratospheric aerosols in the post-Pinatubo period measured by the occultation radiometer experiment ORA, *Atmos. Environ.*, *35*, 5067–5078.
- Fussen, D., F. Vanhellemont, and C. Bingen (2001b), Evidence of transport, sedimentation and coagulation mechanisms in the relaxation of post-volcanic stratospheric aerosols, *Ann. Geophys.*, *19*, 1157–1162.
- Goodman, J., K. G. Snetsinger, R. F. Pueschel, G. V. Ferry, and S. Verma (1994), Evolution of Pinatubo aerosol near 19 km altitude over western North America, *Geophys. Res. Lett.*, *21*, 1129–1132.
- Hitchman, M. H., M. McKay, and C. R. Trepte (1994), A climatology of stratospheric aerosol, *J. Geophys. Res.*, *99*, 20,689–20,700.
- Hofmann, D. J. (1988), Aerosols from past and present volcanic emissions, in *Aerosols and Climate*, edited by V. Hobbs and M. P. McCormick, pp. 195–214, A. Deepak, Hampton, Va.
- Holton, J. R. (1992), *An Introduction to Dynamic Meteorology*, *Int. Geophys. Ser.*, vol. 48, 3rd ed., Academic, San Diego, Calif.
- Lambert, A., R. G. Grainger, C. D. Rodgers, F. W. Taylor, J. L. Mergenthaler, J. B. Kumer, and S. T. Massie (1997), Global evolution of the Mt. Pinatubo volcanic aerosols observed by the infrared limb-sounding instruments CLAES and ISAMS on the Upper Atmosphere Research Satellite, *J. Geophys. Res.*, *102*, 1495–1512.
- Pueschel, R. F., B. Russell, D. A. Allen, G. V. Ferry, and K. G. Snetsinger (1994), Physical and optical properties of the Pinatubo volcanic aerosol: Aircraft observations with impactors and a Sun-tracking photometer, *J. Geophys. Res.*, *99*, 12,915–12,922.
- Randall, C. E., R. M. Bevilacqua, J. D. Lumpe, K. W. Hoppel, D. W. Rusch, and E. P. Shettle (2000), Comparison of Polar Ozone and Aerosol Measurement (POAM) II and Stratospheric Aerosol and Gas Experiment (SAGE) II aerosol measurements from 1994 to 1996, *J. Geophys. Res.*, *105*, 3929–3942.
- Renard, J.-B., et al. (2002), Optical and physical properties of stratospheric aerosols from balloon measurements in the visible and near-infrared domains. II. Comparison of extinction, reflectance, polarization, and counting measurements, *Appl. Opt.*, *36*, 7540–7549.
- Russell, P. B., et al. (1996), Global to microscale evolution of the Pinatubo volcanic aerosol, derived from diverse measurements and analyses, *J. Geophys. Res.*, *101*, 18,745–18,763.
- Stein, B., M. Del Guasta, J. Kolenda, M. Morandi, P. Rairoux, L. Stefanutti, J. P. Wolf, and L. Wöste (1994), Stratospheric aerosol distribution from multispectral lidar measurements at Sodankylä during EASOE, *Geophys. Res. Lett.*, *21*, 1311–1314.
- Stone, R. S., J. R. Key, and E. G. Dutton (1993), Properties and decay of stratospheric aerosols in the Arctic following the 1991 eruptions of Mount Pinatubo, *Geophys. Res. Lett.*, *20*, 2359–2362.
- Sugita, T., Y. Kondo, M. Koike, M. Kanada, N. Toriyama, and H. Nakajima (1999), Balloon-borne optical counter for in situ aerosol measurements, *J. Atmos. Chem.*, *32*, 183–204.
- Thomason, L. W., L. R. Poole, and T. Deshler (1997), A global climatology of stratospheric aerosol surface area density deduced from Stratospheric Aerosol and Gas Experiment II measurements: 1984–1994, *J. Geophys. Res.*, *102*, 8967–8976.
- Tie, X., X. Lin, and G. Brasseur (1994), Two-dimensional coupled dynamical/chemical/microphysical simulation of global distribution of El Chichón volcanic aerosols, *J. Geophys. Res.*, *99*, 16,779–16,792.
- Trepte, C. R., L. W. Thomason, and G. S. Kent (1994), Banded structures in stratospheric aerosol distributions, *Geophys. Res. Lett.*, *21*, 2397–2400.
- van de Hulst, H. C. (1957), *Light Scattering by Small Particles*, Dover, Mineola, N. Y.
- Weisenstein, D. K., G. K. Yue, M. K. W. Ko, D.-N. Sze, J. M. Rodriguez, and C. J. Scott (1997), A two-dimensional model of sulfur species and aerosols, *J. Geophys. Res.*, *102*, 13,019–13,035.
- Zhao, J., R. P. Turco, and O. B. Toon (1995), A model simulation of Pinatubo volcanic aerosols in the stratosphere, *J. Geophys. Res.*, *100*, 7315–7328.

C. Bingen, D. Fussen, and F. Vanhellemont, Belgian Institute for Space Aeronomy (IASB-BIRA), 3 avenue Circulaire, B-1180 Brussels, Belgium. (christine.bingen@oma.be; didier.fussen@oma.be; filip.vanhellemont@oma.be)

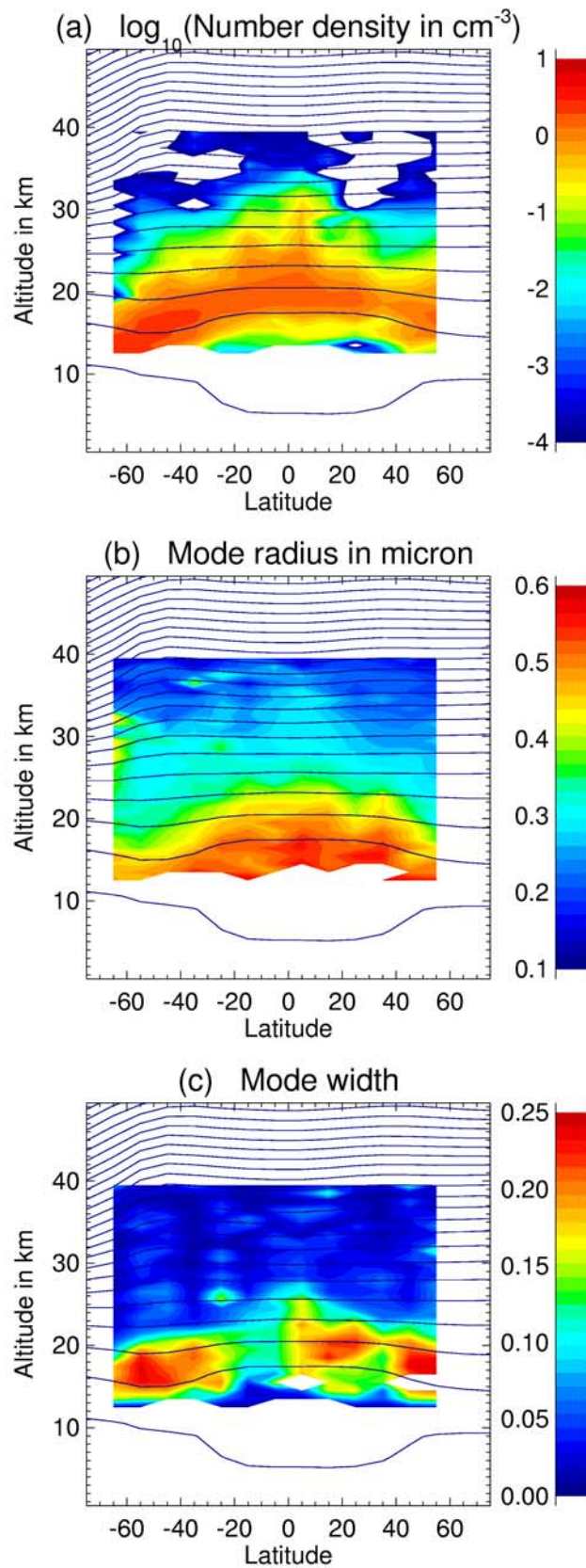


Figure 1. Mean dependence in latitude and altitude of the three aerosol parameters of interest, for September 1993: (a) particle number density, (b) median radius, and (c) mode width. The contour lines represent isentropic lines.

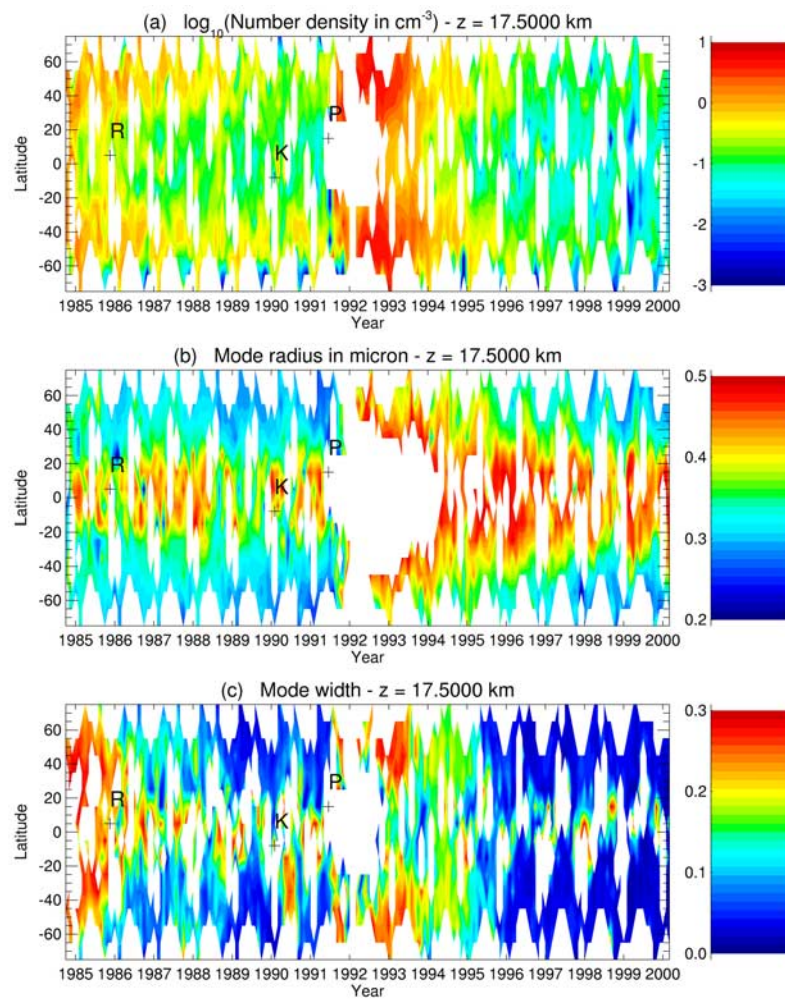


Figure 2. Mean dependence in time and latitude of the aerosol parameters of interest, at $z = 17.5$ km: (a) particle number density, (b) median radius, and (c) mode width.

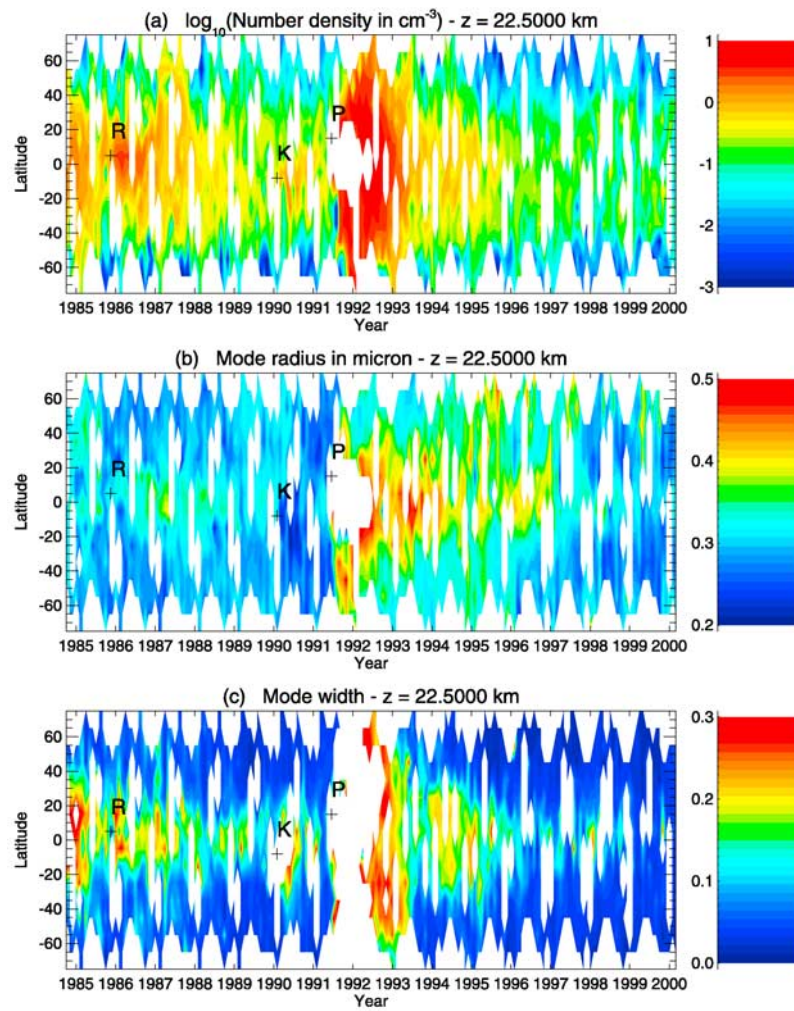


Figure 3. Same as Figure 2, at $z = 22.5 \text{ km}$.

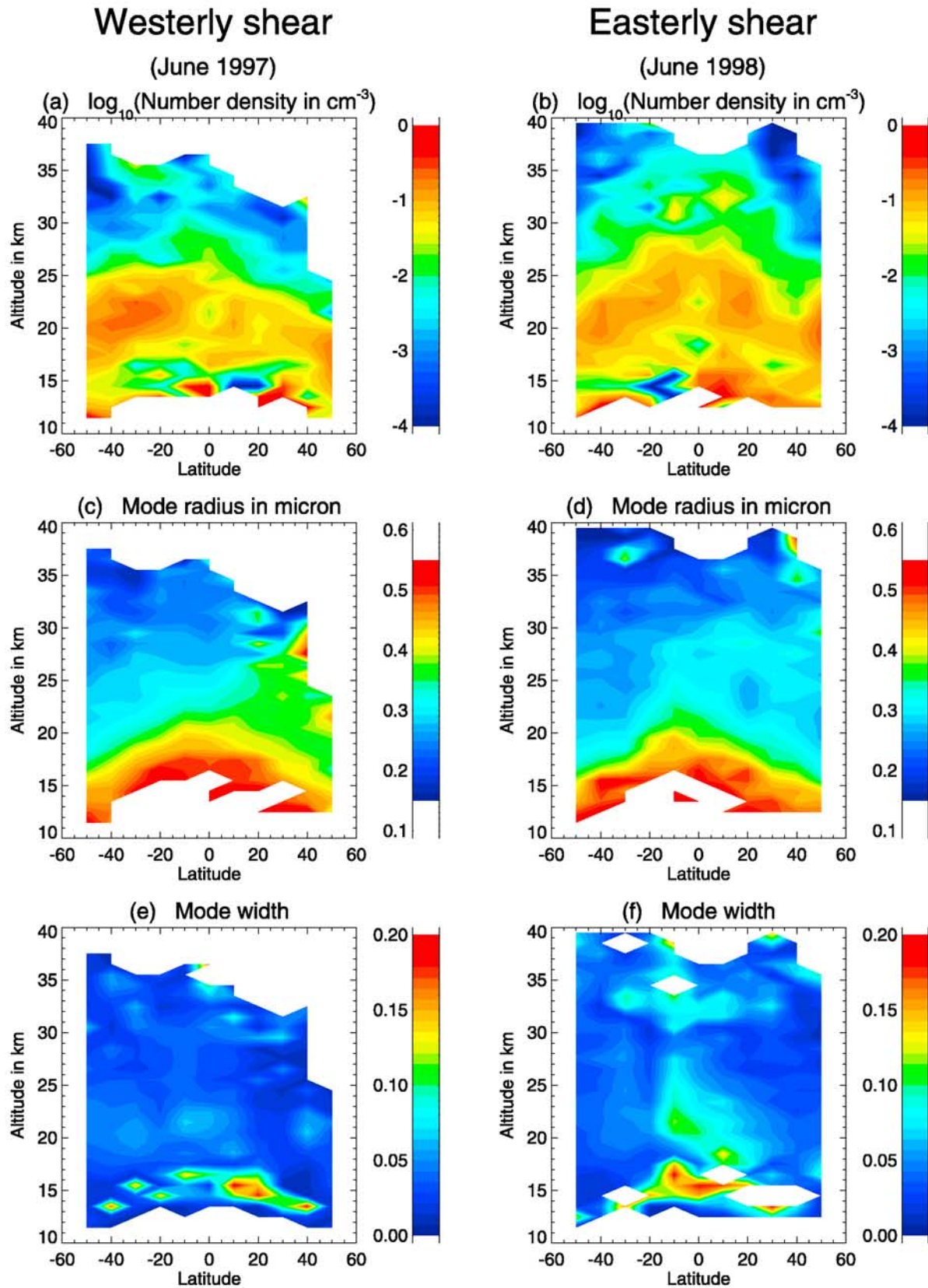


Figure 4. Influence of the QBO on the aerosol parameter profiles. (a and b) $\text{Log}_{10}(N)$; (c and d) median radius; (e and f) mode width. The profiles concern the months June 1997 and June 1998, taking place in two consecutive phases of the QBO, respectively the westerly and easterly shear.